

# Heat accumulation in microdrilled glass from ultraviolet laser ablation

Hirofumi Hidai<sup>1</sup> · Souta Matsusaka<sup>1</sup> · Akira Chiba<sup>1</sup> · Noboru Morita<sup>1</sup>

Received: 28 January 2015 / Accepted: 20 April 2015 / Published online: 26 April 2015  
© Springer-Verlag Berlin Heidelberg 2015

**Abstract** We present numerical and experimental studies of heat accumulation during high-aspect-ratio ultraviolet laser microdrilling of glass. The dependence on pulse repetition rate of the ablation threshold was studied. The rate determines the amount of heat accumulation and temperature variation across the illuminated area. No change in the glass was observed for pulse energies below 1  $\mu\text{J}$  at 1 kHz; melting occurred at 0.3  $\mu\text{J}$ , with ablation at 0.7  $\mu\text{J}$  at 20 kHz. Also, the hole depth doubled when the pulse repetition rate was increased from 1 to 20 kHz. Moreover, the fluence of  $\sim 4 \text{ J/cm}^2$  that passed through drilled holes at 1 kHz decreased to  $\sim 1 \text{ J/cm}^2$  at 20 kHz.

## 1 Introduction

Laser microdrilling of a material involves using multiple pulses of laser illumination which melts and ablates the material and thereby results in a hole being drilled [1–7]. When these pulses illuminate the surface at high repetition rates, each successive pulse is illuminating an area heated by previous pulses before the area has had time to cool down. Therefore, because the illuminated area is already heated, laser illumination at high repetition rate enables melting and ablation to proceed with just low-energy pulses. This process yields reduced ablation thresholds [3, 7] and drilling speed enhancement [2].

There have been previous reports on the effect of heat accumulation in illuminated materials. Ancona et al. [2]

drilled through stainless steel and copper plates using femtosecond-pulsed lasers and reported drilling speed enhancements with increasing repetition rates in the range from 50 to 975 kHz. Brygo et al. [3] measured and estimated the temperature at workpiece surfaces using a one-dimensional temperature model and reported a reduction in ablation threshold. Finger et al. [5] reported on the heat accumulation and pulse–particle interactions occurring during percussion drilling of steel. They clarified the ablation rate dependence of the repetition rate. Hiramoto et al. [4] drilled SiC and poly(methyl methacrylate) with a CO<sub>2</sub> laser and reported the pulse repetition rate at which heat accumulation begins to occur and its influence on the drilled hole shape. Weber et al. [8] studied the geometry of the laser heat source and temperature fields comparing three-dimensional and one-dimensional heat flows using the results obtained from microhole drilling of stainless steel and the cutting of anisotropic materials, e.g., carbon fiber-reinforced plastics (CFRP). Many studies on heat accumulation in glass have been reported [9–13]; the transparency of glass enables inside focusing and modification induced by ultrafast laser illumination. The modification can be applied for machining after etching [10], waveguide formation [11], and welding [12, 13].

Deep laser drilling is a challenging task because of difficulties in ejecting ablated material from the hole, in eliminating plasma shielding in the hole, and in delivering energy to the bottom of the hole. Defocusing occurs as the drilling progresses and causes a reduction in the energy density. Studies of deep drilling, for example, monitoring of on-line depth [14] and hole-shape evolution [15, 16], and the effects of particle shielding and heat accumulation on drilling speed [2, 5] were conducted.

The solution of these problems using the ablation threshold reduction caused by heat accumulation is

✉ Hirofumi Hidai  
hidai@faculty.chiba-u.jp

<sup>1</sup> Department of Mechanical Engineering, Chiba University,  
1-33 Yayoi-cho, Inage-ku, Chiba 263-8522, Japan

expected to lead to better deep-hole drilling. Much has been reported on the ablation threshold; however, to the best of the authors' knowledge, there are no reports about the relationship between hole depth and ablation threshold reduction caused by heat accumulation within the illuminated material.

By exploiting its transparency, deep laser drilling in glass can be viewed and analyzed. With the laser beam focused on the front surface, filamentation-assisted laser drilling can be analyzed as well [17, 18]. The laser beam can be focused through the bulk sample onto the rear surface and hence the beam energy can be transferred to the rear surface [19–21]. Microchannel forming in glass using a focused femtosecond laser beam and selective chemical etching has been reported [10, 22]. In contrast, deep drilling from the front surface has had less attention as such drilling is difficult to achieve.

In this study, we have demonstrated that the ablation threshold reduction caused by heat accumulation enables high-aspect-ratio microdrilling in glass, and we shall report on the correlation between pulse repetition rate and heat accumulation. We remark that measuring the pulse energy and the beam profile at the bottom of the hole is difficult and differs from that at the surface because of reflections occurring at the surface of the hole interior [1]. We first studied experimentally and numerically the dependence on pulse repetition frequency of the ablation threshold at the glass surface. The pulse repetition dependence of the hole depth and of the fluence that passes through the drilled hole is then analyzed, and results are discussed.

## 2 Experimental methods

Because plasma absorption becomes stronger at longer wavelengths [23] and the focal depth is large, a short-wavelength laser source is effective in reducing plasma shielding. Therefore, an ultraviolet (UV) laser (DS20H-266, Photonics Industries International, Inc., Bohemia, NY) operating at a wavelength of 266 nm was used. After passing the laser beam through a quarter-wave plate, a circularly polarized focused beam is produced and used for illumination. The beam was then focused on the sample using a convex lens with focal length of 30 mm. No relative scanning of the laser beam was performed during illumination. In our study, the laser was operated with pulse repetition rates ranging from 1 to 20 kHz and with pulse widths ranging from 8 to 9 ns (depending on the repetition rate; 8 ns at <15 kHz and 9 ns at 20 kHz). Side-view shadowgraph images under white-light illumination were obtained for process monitoring.

The samples used were of glass with common compositions, e.g., borosilicate glass. During testing though,

cracks formed inside the glass from the illumination at pulse energies close to the ablation threshold. To mitigate cracking, a short-wave cutoff filter (SCF-50S-38L, Sigma Koki Co., Ltd., Saitama, Japan) with composition similar to BK7 was used during surface ablation because its transmissivity is low; no cracking appeared inside the glass irrespective of conditions. We used filter thicknesses of 0.18, 3.0, and 8.0 mm. The glass transition point and deformation point of the filter are 753 and 808 K, respectively [24]. The composition of the filter was obtained by energy-dispersive X-ray spectrometry. The result indicated traces of Pb in addition to the elements Si, O, B, Na, K, and Ba that comprise BK7. A 10-mm-thick borosilicate glass (Pyrex<sup>®</sup>, Corning 7440, Corning Inc. Corning, NY) was also tested in drilling at high laser energies.

The absorption coefficients for the short-wave cutoff filter and borosilicate glass were measured using thin samples obtained by grinding and polishing. Transmissivity was measured using a spectrophotometer (V-550, JASCO International Co., Ltd., Tokyo, Japan). The result for the transmissivity of the filter (thickness of 0.18 mm) was <0.1 % at wavelengths from 200 to 356 nm, and the transmissivity of borosilicate glass (thickness of 0.1 mm) was 37 % at the wavelength of 266 nm. Assuming the surface reflection of the filter and glass is 4 %, the respective absorption coefficients of the filter and glass are >370 and 90 cm<sup>-1</sup> at the wavelength of 266 nm.

## 3 Calculations

Numerical calculations were performed to estimate the temperature of the glass. Because the illuminated area was cylindrically symmetrical around the optical axis, we employed a two-dimensional model of the temperature variation  $T(t, z, r)$  over a square area described in terms of the cylindrical coordinates  $r$  and  $z$ . The heat equation is then given as [25, 26]

$$c\rho \frac{\partial}{\partial t} T(t, z, r) = k \left[ \frac{\partial}{\partial z^2} T(t, z, r) \right] + \frac{1}{r} \frac{\partial}{\partial r} \left[ rk \left( \frac{\partial}{\partial r} T(t, z, r) \right) \right] + Q(t, z, r). \quad (1)$$

where  $z$  is the coordinate along the optical axis,  $r$  the radial coordinate,  $c$  the specific heat,  $k$  the thermal conductivity,  $\rho$  the density of the glass used, and  $Q$  the absorbed heat source. Calculations at high temperatures above the boiling point are challenging because one must consider heat-induced evaporation, heat radiation, evaporated particle shielding, and the temperature dependencies of many material constants. Therefore, we focused on modeling of the temperature variation below  $\sim 1000$  K and compared

results with those from the heat-affected zone. The specific heat, the thermal conductivity, and the density are assumed to be constant. The initial temperature was taken to be 293 K. The origin was set at the center of the laser spot on the surface. Calculations were performed for a square area, with depth and radius of 150 μm, over which constant-temperature conditions were applied. We assumed an absence of heat sinks on the surface of the glass as the thermal conductivity of air is much less than that of glass.

The radiation intensity  $I$  is taken to have a Gaussian profile with a spot radius  $\omega$  of 7.3 μm ( $1/e^2$  spot), which is calculated from the specifications of the laser and the focal length. Surface absorption was assumed. The heat source is expressed as

$$Q(t, z, r) = \begin{cases} \frac{\partial}{\partial z}(1 - R)I(t, r) & (z = 0), \\ 0 & (z \neq 0) \end{cases}, \tag{2}$$

with

$$I(t, r) = \begin{cases} \frac{2P}{\pi\omega^2} \exp\left(\frac{-2r^2}{\omega^2}\right) & \left(\frac{n}{f} \leq t \leq \frac{n}{f} + \tau\right) \quad n = 0, 1, 2, \dots \\ 0 & (\text{otherwise}) \end{cases} \tag{3}$$

Here,  $P$  is the laser power and  $f$  the pulse repetition rate. The reflectivity of the glass  $R$  is set to 0.1 without any dependence on temperature. The pulse width  $\tau$  is set to 8 ns. Equations (1)–(3) are solved by the finite-difference method using a uniform  $r$  and  $z$  meshes with mesh step sizes  $\Delta r$  and  $\Delta z$  of 1 μm. The time step  $\Delta t$  is set at 8 ns, which is the same as the laser pulse width. Therefore, the heat flux is inputted in single time steps with rates ranging from 1 to 20 kHz to match the experimental conditions. The numerical calculation ignored the temperature dependencies of the material constants: that is, specific heat, thermal conductivity, and density. The calculations involving Eqs. (1) and (2) use the following values [27]:  $\rho = 2.51 \text{ g/cm}^3$ ,  $c = 0.858 \text{ J/g K}$ , and  $k = 0.0111 \text{ W/cm K}$ .

## 4 Results and discussion

### 4.1 Surface ablation experiment

Figure 1 shows the surface of the short-wave cutoff filter after 1000 pulses of laser illumination set approximately at the threshold energy for melting and ablation. No changes were observed when the laser energy and the pulse repetition rate were small (energy of  $<1 \mu\text{J}$  for repetition rate of 1 kHz). A heat-affected zone (i.e., a softened zone) was observed (energy of  $0.5 \mu\text{J}$  for repetition rates of 10 and 20 kHz) that increases with laser energy, and then

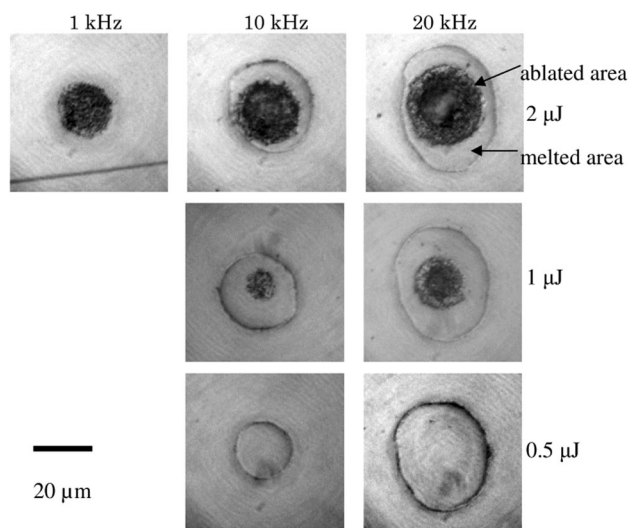


**Fig. 1** Micrographs of laser illuminated spots for various pulse repetition rates and pulse energies. The number of pulses used was 1000 pulses. The filter thickness was 3 mm. Ablated craters are observed at the centers when pulse energies are  $>1 \mu\text{J}$ , and melted zones are observed when pulse repetition rates are 10 and 20 kHz. No changes are observed when the repetition rate was 1 kHz and the pulse energy was below  $1 \mu\text{J}$

ablated areas were observed (for energy of  $2 \mu\text{J}$  with a repetition rate of 1 kHz and for energies  $>1 \mu\text{J}$  with repetition rates of 10 and 20 kHz).

The results from illuminations at various repetition rates and laser energies are summarized in Fig. 2. For a pulse repetition rate of 1 kHz, no changes were observed when laser energies was below  $1 \mu\text{J}$ . Ablated craters were observed when the laser energy was above  $1.2 \mu\text{J}$ . In contrast, for a pulse repetition rate of 20 kHz, a melted area was observed at pulse energies above  $0.3 \mu\text{J}$ , and ablated craters were observed at pulse energies above  $0.8 \mu\text{J}$ . Therefore, the ablation threshold is reduced by approximately

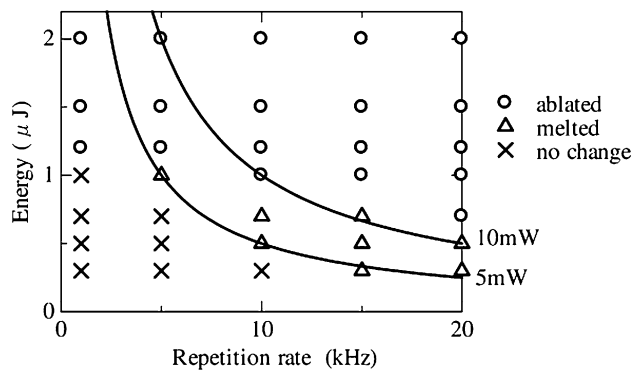


**Fig. 2** Laser illumination results for various repetition rates and pulse energies. The number of pulses used was 1000 pulses. *Open circle*: ablated crater is observed; *open triangle*: ablated crater is not observed, but melting is observed; *cross*: no change is observed

one half by increasing the pulse repetition rate from 1 kHz to 20 kHz. This is believed to be a result of heat accumulation. Specifically, slow repetition rates allow sufficient time between successive pulses for heat to diffuse away from the focal volume. Fast repetition rates allow heat to accumulate in the illuminated area, and hence less energy is needed to maintain the softening of the illuminated material and boiling point. Therefore, heat-affected and ablation zones at a reduced pulse energy and higher repetition rate were observed. In Fig. 2, contours representing average power have been drawn, and the boundaries between “no change observed” (marked with crosses) and “heat-affected zone recognized” (marked with open triangles) and between “heat-affected zone recognized” and “ablation observed” (marked with open circles) roughly correspond with the lines indicating laser powers of 5 and 10 mW, respectively, when the laser energy is  $<1 \mu\text{J}$ . Heat-affected zones and ablation were observed at lower average powers for pulse energies of more than  $1 \mu\text{J}$ .

The difference arises because the pulse energy is large enough to cause ablation with a single pulse.

#### 4.2 Numerical calculation

To estimate the temperature distribution, numerical calculations were performed. Figure 3 shows this distribution after the first pulse illumination for an area  $50 \mu\text{m}$  in depth from the surface and  $50 \mu\text{m}$  in radius from the optical axis. The calculated area was  $150 \mu\text{m}$  in depth from the surface and  $150 \mu\text{m}$  in radius from the optical axis, but the figure was trimmed to show more clearly the temperature distribution around the illuminated area. Only the material around the surface is heated after the first pulse illumination (Fig. 3a), and the heat diffuses out of the focal volume and into the glass. The temperature at the surface was  $\sim 570 \text{ K}$  (the temperature rise being  $\sim 280 \text{ K}$ ) after  $50 \mu\text{s}$  (b) and decreased to  $\sim 297 \text{ K}$  (temperature rise being  $\sim 4 \text{ K}$ ) after  $1 \text{ ms}$  (f). These intervals correspond to

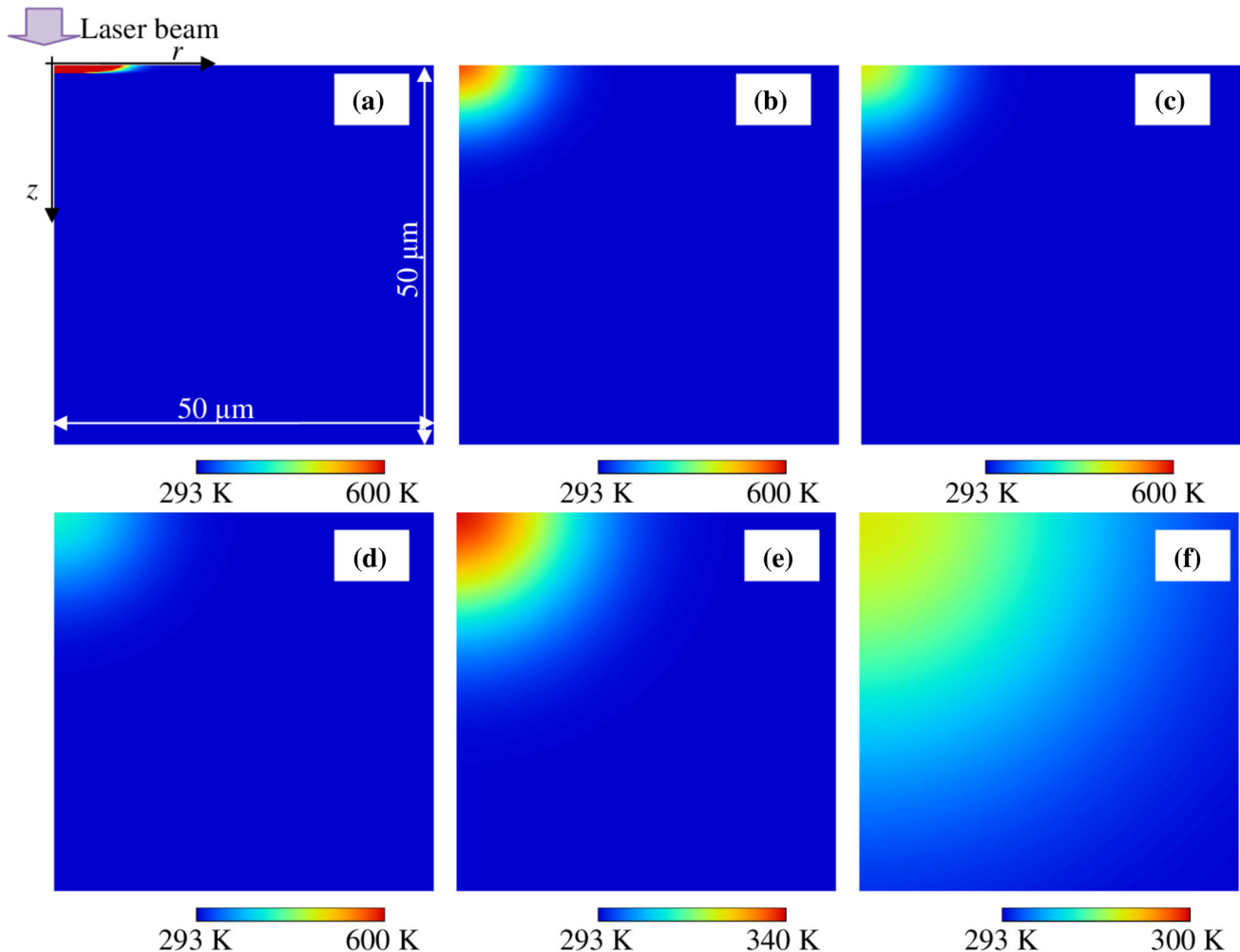
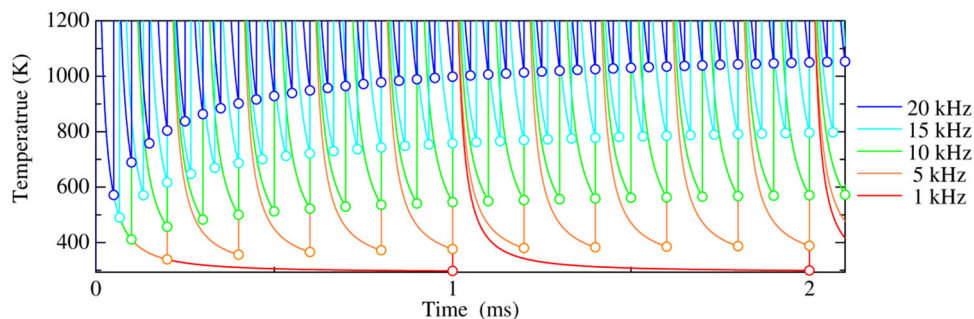


**Fig. 3** Simulated temperature of the glass **a** 8 ns, **b** 50  $\mu\text{s}$ , **c** 67  $\mu\text{s}$ , **d** 100  $\mu\text{s}$ , **e** 200  $\mu\text{s}$ , and **f** 1000  $\mu\text{s}$  after first pulse illumination. The illustrated area is  $50 \mu\text{m}$  in the  $r$  axis and  $50 \mu\text{m}$  in the  $z$  axis

**Fig. 4** Calculated temperatures at the center of the laser spot. The laser energy was  $1 \mu\text{J}$



successive pulse illuminations at repetition rates of 20 and 1 kHz.

The calculated temperature at the center of the surface where the hottest spot occurs is presented in Fig. 4. When illumination of the surface begins, the temperature rises, peaks, and then cools gradually. Successive illumination pulses then cause repeated temperature increases. With a 1-kHz repetition rate, i.e., a laser pulse illumination every 1 ms, the temperature decreases to  $\sim 297$  K by the time that the second pulse begins. In contrast, for laser illuminations of higher repetition rates, successive pulses illuminate the surface before it has a chance to cool, and raises the temperature with every pulse.

To analyze the heat accumulation over longer time durations, the temperatures just before each laser pulse begins (indicated by open circles in Fig. 4) are plotted in Fig. 5. The figure shows the temperatures up to the 1000th pulse for each of the pulse repetition rates. For all rates, the temperature increases rapidly for the first 5 ms; afterward the increments decrease until the temperature is almost constant after 20 ms. The temperature is above 1100 K after 10 ms under illumination with the 20-kHz repetition rate, whereas the temperature is only  $\sim 300$  K for the 1-kHz repetition rate. That is, the surface temperature increases with higher repetition rates. Therefore, laser illuminations with higher repetition rates produce heat accumulations, the formation of heat-affected zones, and the reduction in the ablation threshold.

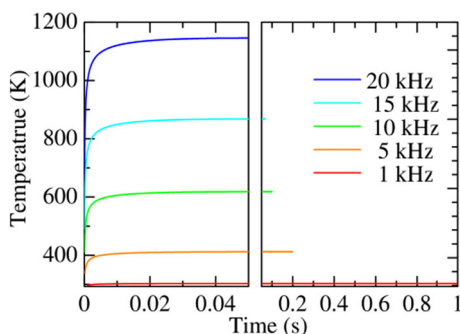
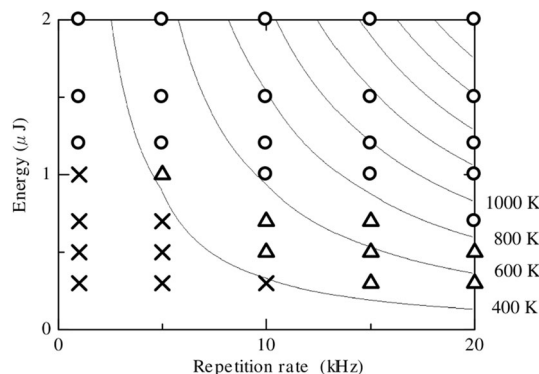


**Fig. 5** Temperature evolution at the center of the laser spot during laser irradiation at different repetition rates up to 1000 pulses. The laser energy was  $1 \mu\text{J}$

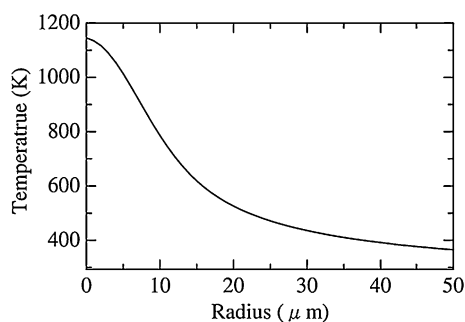
Figure 6 shows contour lines for the temperature just before the 1000th pulse illumination for various pulse energies and pulse repetition rates. The experimental results shown in Fig. 2 are also plotted in Fig. 6. Temperatures of between 400 and 600 K for the heat-affected zone correspond well with those observed experimentally. The transition point of the short-wave cutoff filter is  $\sim 750$  K [24] (working temperature and boiling point of the short-wave cutoff filter were not available). The calculated temperature at the observed heat-affected zone was lower than the glass transition point. This is explained from the fact that the plotted temperatures shown are taken at times just before the 1000th pulse illumination, when the temperature varies rapidly above the temperature plotted in Fig. 6.

Figure 7 shows the surface temperature distribution at the same number of pulses as that of Fig. 6. The pulse energy is  $1 \mu\text{J}$ , and the pulse repetition rate is 20 kHz. The temperature at the center is  $\sim 1150$  K. In Fig. 1, a heat-affected zone with a radius of  $18 \mu\text{m}$  is observed under the same conditions. From the calculations, the temperature is  $\sim 550$  K at a radius of  $18 \mu\text{m}$ , and the results here show that this result corresponds well with those shown in Fig. 6.

Material properties at high temperatures are not available. Therefore, this calculation ignores the temperature dependences of the material constants, as well as heat of evaporation, heat radiation, and heat conduction to the atmosphere; the actual temperature is therefore believed to



**Fig. 6** Temperature at the center of the laser spot just before illumination by the 1000th pulse



**Fig. 7** Temperature distribution at the surface just before illumination by the 1000th pulse. The repetition rate was 20 kHz, and the pulse energy was 1  $\mu\text{J}$

be lower than the calculated results, and these assumptions cause large errors at high temperatures. The analysis of the ablation threshold therefore does not use this calculation; however, this error was not large at lower temperatures, and the calculated softening phenomena matched the experimental results. From these observations, it was confirmed both experimentally and numerically that the pulse repetition rate governs heat accumulation and temperature.

In other research [5, 8, 11, 28], the material constants were also assumed to be constant. Hence, our calculated temperatures can be compared with those related research reports. Guttas et al. [28] studied the effects of heat accumulation in soda-lime glass by focusing bursts of femtosecond laser pulses at various repetition rates. They found that the threshold for changes in the glass phase due to heat accumulation corresponds to the time interval for which the temperature at the focus increases by  $150 \pm 50$  K between successive bursts under pulse repetition rates of 0.2–2.5 MHz.

In our result, the temperature increment just before the second pulse illumination begins (the time corresponding to the first open circle marked in Fig. 4) was 55–140 K under laser illumination conditions when only heat accumulation effect (marked by triangles in Fig. 2) was observed. The temperature values were  $\sim 50$  K smaller than that reported by Guttass et al. [28]. Moreover, in our experiment, the pulse repetition rate (20 kHz) was at least 10 times slower than that reported by Guttass et al. Longer pulse intervals produced extended heated area around the laser spot, because such pulses are able to heat larger areas and enable heat to accumulate with smaller temperature increments after each pulse. Changes in pulse repetition rate determined different temperature increments after each pulse.

### 4.3 Repetition rate dependence of hole depth

Deep drilling in a short-wave cutoff filter was performed at higher laser energies. Thermal shock causes cracks around

the holes with such illumination energies ( $> \sim 30$   $\mu\text{J}$ ). Tests with various laser powers indicate an energy of 10  $\mu\text{J}$  below which the short-wave cutoff filter remained crack free. The fluence at the surface was calculated to be  $\sim 6.1$   $\text{J}/\text{cm}^2$ . Figure 8 shows some typical results. The hole depth varied with pulse repetition rate. At the pulse repetition rate of 20 kHz, the hole depth is  $\sim 500$   $\mu\text{m}$ . The diameter around the entrance of the hole is  $\sim 25$   $\mu\text{m}$ , and this diameter decreases with hole depth. In particular, the hole diameter is  $\sim 8$   $\mu\text{m}$  at a depth of  $\sim 130$   $\mu\text{m}$ . The diameter is then almost constant between depths of  $\sim 130$  and  $\sim 500$   $\mu\text{m}$  (the bottom of the hole); the aspect ratio

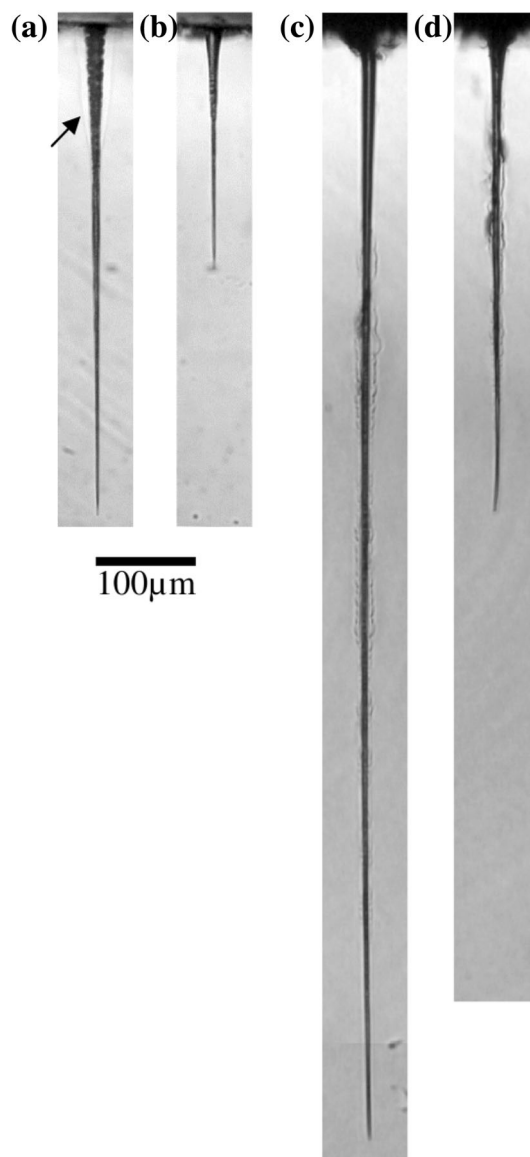


**Fig. 8** Transverse cross section and profile of the drilled hole in **a**, **b** the short-wave cutoff filter and **c**, **d** borosilicate glass. Thickness of the filter and borosilicate glass was 8 and 10 mm, respectively. The pulse energy is **a**, **b** 10  $\mu\text{J}$  and **c**, **d** 30  $\mu\text{J}$ , the number of pulses was 5000, and the repetition rates were **a**, **c** 20 kHz, and **b**, **d** 1 kHz

(depth/diameter) is then  $\sim 45$  in this depth range. In contrast, the hole depth is  $\sim 250 \mu\text{m}$  for the 1-kHz pulse repetition rate. Deeper holes were not able to be drilled, even if the total number of pulses was increased given a specific pulse repetition rate. Therefore, the fluence at the bottom of the holes was less than the glass ablation threshold, because the laser energy dissipates through defocusing and propagation within the thin holes.

The heat-affected zone is observed around the hole from the surface down to a depth of  $\sim 150 \mu\text{m}$  (indicated by an arrow in Fig. 8a). This zone becomes narrower with hole depth because, as the hole became deeper, the laser energy delivered to the bottom of the hole decreases through defocusing and dissipation. The result at the 1-kHz repetition rate, for which no modified zone is observed, corresponds with the result shown in Fig. 1.

Drilling in borosilicate glass was also tested. Cracks appeared in the glass interior for pulse energies set below  $\sim 10 \mu\text{J}$ ; ablation from the surface occurred with pulse energies set above  $30 \mu\text{J}$ . Hence, drilling was tried with a pulse energy of  $30 \mu\text{J}$ . Typical results are shown in Fig. 8. The depth of the holes is  $\sim 1120 \mu\text{m}$  at 20 kHz and  $\sim 500 \mu\text{m}$  at 1 kHz. The holes drilled went no deeper, even when the total number of pulses was increased.

Three holes are drilled in the short-wave cutoff filter under the same conditions, and the average depths are plotted for various repetition rates (Fig. 9a) and numbers of pulses (Fig. 9b). The holes become deeper with increasing

numbers of pulses. The hole depths are saturated after 1000 pulses for repetition rates 1 and 5 kHz and are saturated after 2000 pulses for repetition rates 10, 15, and 20 kHz. Hole depth increases linearly up to 500 pulses, that is, the ablation rate is almost constant; hole depth increases slightly with increasing repetition rate for pulse numbers below 500, i.e., the averaged ablation rate increases slightly with increasing pulse repetition rate.

However, hole depth after sufficient pulse illuminations to terminate drilling (2000 pulses in Fig. 9) depends on the pulse repetition rate. In particular, the hole depth is  $\sim 250 \mu\text{m}$  for a pulse repetition rate of 1 kHz and depth  $\sim 500 \mu\text{m}$  for a repetition rate of 20 kHz. The pulse repetition rate dependence is believed to be a result of the reduction in the ablation threshold by heat accumulation. The hole depth in borosilicate glass increased with increasing pulse repetition rate in the same manner as for the short-wave cutoff filter.

#### 4.4 Repetition rate dependence on the fluence throughout the holes

The estimation of heat accumulation at the bottom of the hole is a challenge because the beam mode varies as a result of multiple reflections from the inner surface of the hole and because the bottom of the hole is not flat. In this study, the laser energy at the bottom of the hole was estimated from the energy emitted from a through-hole. The through-holes were obtained by drilling into a thin short-wave cutoff filter plate (of thickness  $180 \mu\text{m}$ ). The plate was drilled using beams of different pulse energies. When the laser energy is low, drilling a hole completely through is not possible. Through-holes were produced using slightly larger pulse energies. The laser energy can then be measured with a power meter placed below the through-hole.

Figure 10 plots the fluence that passed through the holes against repetition rate. The bars indicate the fluence required at the surface to drill through the short-wave cutoff filter. These fluences were calculated from the laser energy and calculated spot diameter ( $14.5 \mu\text{m}$ ,  $1/e^2$ ). The through-holes were created using laser fluences that were above levels represented by the bars; no through-holes were created for fluences below these levels. The open squares in Fig. 10 indicate the fluences that were emitted from the through-holes when the laser fluence is at the level represented by the upper edge of the bar. These laser fluences were calculated from the laser energies that passed through and the areas of the holes. Three holes were drilled for each repetition rate. The averaged fluence is indicated by the open square, and the accompanying error bar shows maximum and minimum values. The power was measured after 5000 pulse illuminations, and the transmitted laser energy

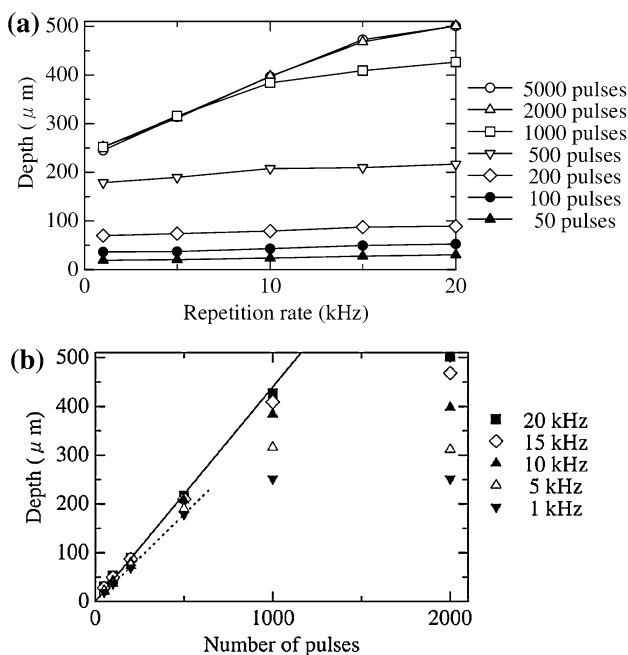


**Fig. 9** Depths of holes drilled with different repetition rates (a) and numbers of pulses (b). The pulse energy was set at  $10 \mu\text{J}$ . *Solid* and *dotted* line in (b) are fit with 20- and 1-kHz repetition rates, respectively, for 50–500 pulses

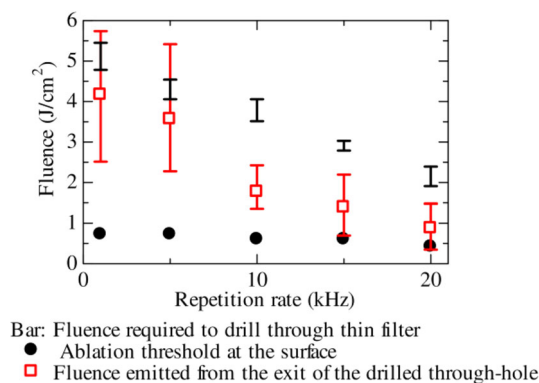


**Fig. 10** Fluence required to drill through filter and the fluences within the drilled holes for various repetition rates. The thickness of the filter was 0.18 mm. *Bar*: fluence required to drill through a thin filter; *open square*: fluence emitted from the drilled through-hole with *error bars* indicating maximum and minimum values; *closed circle*: ablation threshold at the surface

remained constant. In the figure, the ablation thresholds at the surface are marked with closed circles (calculated from the data shown in Fig. 2). These results show that the fluences required at the surface to drill through the short-wave cutoff filter decrease with increasing repetition rates. These results correspond with those of Fig. 9, which show that the final depth of the drilled hole increases with increasing pulse repetition rate. The fluence of  $\sim 4 \text{ J/cm}^2$  for a pulse repetition rate of 1 kHz decreased to  $\sim 1 \text{ J/cm}^2$  for a pulse repetition rate of 20 kHz. These fluences were slightly higher than the threshold required to ablate the short-wave cutoff filter at the bottom of the hole, because the pulse energy was set slightly higher than the threshold required to drill through the filter. This reduction in the ablation threshold at the bottom of each hole enables deeper drilling when using the same energy (as seen in Fig. 9) and enables a reduction in energy required to drill a hole to the same depth (Fig. 10).

In Fig. 10, the fluences that were emitted from the through-holes (red bars) exceeded the required fluences at the surface to drill through the filter (black bars). The reason for this difference is a consequence of the measured area. The surface fluences were calculated from the laser energy and calculated spot diameter ( $14.5 \mu\text{m}$ ). In contrast, the through-hole fluences were calculated from the laser energy that is able to pass through and the sizes of the hole exits. Their diameters were  $1.0\text{--}2.5 \mu\text{m}$ . The fluences were hence calculated with a smaller area around the center of the beam where the fluence was large. Therefore, through-hole fluences exceeded the surface fluences.

The reasons why the fluences calculated at the bottom (open squares in Fig. 10) are larger than fluences at the surface (closed circles in Fig. 10) are explained as follows. As seen in Fig. 8, the bottom of the hole is not flat, and thus the incident angle of the laser beam on the inner surface is

larger than that at the surface. However, the calculated fluences plotted in Fig. 10 do not include the dependence on the angle of incidence, and the sizes of the holes were pre-assumed to have been measured perpendicular to the optical axis. Another reason for the difference is that the fluences at the bottom are calculated based on the hole size ( $1\text{--}3 \mu\text{m}$  in diameter), whereas at the surface, the spot diameter ( $14.5 \mu\text{m}$ ) was used for the calculation.

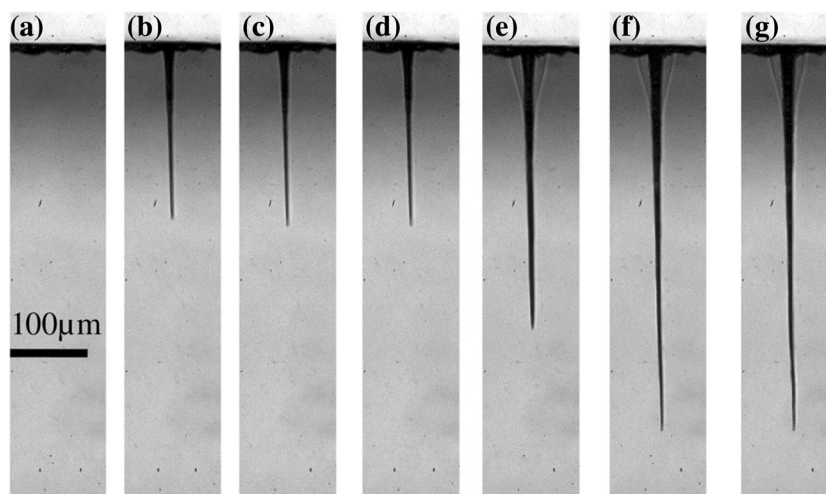
On changing the repetition rate from 1 to 20 kHz, the ablation threshold at the surface fell from  $1.2$  to  $0.8 \mu\text{J}$  at the surface (a 33 % decrease). The threshold for drilling through the short-wave cutoff filter decreased from  $4.2 \mu\text{J}$  to  $0.9 \mu\text{J}$  (a  $\sim 79$  % decrease). The main reasons for the difference in the ablation threshold reductions are the following. For surface absorption, the threshold fluence to initiate ablation was estimated; however, for drilling, the fluence was dominated by the threshold fluence stopping ablation. With material properties depending on temperature, these thresholds were not consistent. In addition, the accumulated heat at the bottom diffuses radially in all directions except back up the hole. However, the accumulated heat at the surface can only diffuse hemispherically. These differences cause quantitative mismatches.

We then confirmed that an increase in the repetition rate enables deeper drilling to be performed using this method. First, the drilled hole, created with a pulse energy of  $10 \mu\text{J}$  and a repetition rate of 1 kHz, was imaged through the laser drilling apparatus after every 500 pulses. When the hole depth becomes saturated, the repetition rate of illumination was increased to 20 kHz (Fig. 11). A hole with a depth of  $\sim 200 \mu\text{m}$  was obtained after 500 pulses of laser illumination at the pulse repetition rate of 1 kHz (Fig. 11b). After another 500 pulses (total of 1000 pulses, Fig. 11c), the hole became slightly deeper, and after a further 500 pulses (total of 1500 pulses, Fig. 11d), the depth of the hole was unchanged. Therefore, the hole depth becomes saturated at a depth of  $\sim 230 \mu\text{m}$  for the 1-kHz pulse repetition rate. On changing the pulse repetition rate to 20 kHz, the hole became deeper ( $\sim 370 \mu\text{m}$ ) after 500 pulses (total of 1500 pulses at 1 kHz and 500 pulses at 20 kHz, Fig. 11e). After a further 500 pulses (total of 1500 pulses at 1 kHz and 1000 pulses at 20 kHz, Fig. 11f), the hole depth became deeper still ( $\sim 490 \mu\text{m}$ ). The hole depth again becomes saturated after another 500 pulses (total of 1500 pulses at 1 kHz and 1500 pulses at 20 kHz, Fig. 11g). This result indicates that an increased pulse repetition rate can be used to deepen holes.

No heat-affected zone was observed around the entrance for the pulse repetition rate of 1 kHz (Fig. 11d). However, a heat-affected zone was observed below the surface to a depth of  $\sim 70 \mu\text{m}$  for the 20-kHz repetition rate stage (Fig. 11e). The heat-affected zone was observed even when



**Fig. 11** Transverse section and profile of the drilled hole. Thickness of the filter was 8 mm. **a** Before illumination; **b** after 500 pulses, **c** 1000 pulses, and **d** 1500 pulses at the 1-kHz repetition rate; and after **e** 500 pulses, **f** 1000 pulses, and **g** 1500 pulses at the 20-kHz repetition rate, after the initial 1500 pulses at 1 kHz. The pulse energy was 10  $\mu\text{J}$



the hole had already been drilled in the 1-kHz repetition rate stage because the laser illumination heated the inner surface of the drilled hole. The thickness of the heat-affected zone was narrower in comparison with that seen in Fig. 8, in which the heat-affected zone was observed below the surface to a depth of  $\sim 150 \mu\text{m}$ . The reason for this was that the hole drilled at the 1-kHz repetition rate was already present (Fig. 11d).

#### 4.5 Discussion

The filter contains lead and therefore absorbs ultraviolet light; the absorption coefficient is  $>370 \text{ cm}^{-1}$  for wavelengths shorter than 356 nm. Lead glass generally shows high absorption in the UV region [29]. Therefore, the absorption coefficient is higher for the filter than for BK7. The wavelength of the laser (266 nm) was smaller than the absorption edge. This absorption is due to the transition of a valence electron of a network anion to an excited state [30].

In the calculation, surface absorption was assumed. The ablation rate at the 1-kHz pulse repetition rate is  $0.36 \mu\text{m}/\text{pulse}$  (Fig. 9), which is much smaller than spot diameter ( $14.5 \mu\text{m}$ ). The pulse energy was set at  $10 \mu\text{J}$ , and the value was much larger than the ablation threshold of  $1.2 \mu\text{J}$  (Fig. 2). If the value of the absorption coefficient is not high enough for surface absorption, melt or cracks should be observed around the hole (see Fig. 9b). Therefore, the assumption of surface absorption is considered to be adequate.

Ancona et al. [2] drilled stainless steel and copper plates with thicknesses of 0.5 mm. They used an ultrafast laser with a pulse energy of  $30 \mu\text{J}$  and with repetition rates ranging from 50 to 975 kHz. They reported that heat accumulation enhanced the drilling speed in the stainless steel case. However, this effect was not observed in the

drilling of copper. The explanation is based on the difference between the thermal conductivities of the materials.

From our results, the hole depth obtained after 500 pulses (Fig. 9) increased slightly from 179 to  $217 \mu\text{m}$  with increasing pulse repetition rate, i.e., the ablation rate was enhanced slightly. When compared with the results of Ancona et al. [2], both the laser power used and the repetition rate were lower, and thus the enhancement of the ablation rate caused by heat accumulation was slight in our result. However, with sufficient pulse numbers, the final depth of the hole after laser illumination was doubled by increasing the pulse repetition rate from 1 to 20 kHz.

Brygo et al. [3] calculated the amount of heat accumulated in paint and cement when illuminated with a laser. They used a material with thermal conductivity of  $2.7 \text{ W}/\text{m K}$ , a value that is similar to that of the material used in our study. They reported observing heat accumulation under illumination at the repetition rate of 10 kHz that corresponded closely with our results.

Another mechanism that enabled greater hole depths involved using a short-wavelength beam. Short-wavelength beams extend the Rayleigh range  $Z_R$  and reduces plasma shielding. The Rayleigh range is defined as  $Z_R = \pi\omega_0^2/\lambda$ , where  $\omega_0$  is the spot radius and  $\lambda$  the wavelength [31]; for a given spot radius, this range widens with decreasing wavelength. Under our experimental conditions, the Rayleigh range is calculated to be  $620 \mu\text{m}$ .

For ps-laser drilling, imperfections are formed along the side walls of the holes. These imperfections cause changes in the intensity distribution at the bottom of the holes and create multiple ends in the hole [15]. In our experiments, the drilled holes had almost constant diameter; also no imperfections such as bulges were observed. Hole uniformity is one reason that deep holes can be attained.

Ablated particles in the drilling hole scatter the incident laser pulses and reduce the energy delivered to the bottom

of the hole. Ancona et al. [2] reported that the number of pulses required to drill through a stainless steel plate with thickness of 0.5 mm increased for repetition rates above 500 kHz. They concluded that the reduction in drilling efficiency is caused by particle shielding. In our experiment, the repetition rates were set below 20 kHz, which is a factor of 1/25 that used in the experiments by Ancona et al., and the depth of the drilled hole in the filter was  $\sim 0.5$  mm. In addition, the depth of the holes increased with increasing pulse repetition rate. Hence, there was sufficient time for the ablated particle to be ejected from the hole before each subsequent illumination pulse; therefore, particle scattering was not prominent during drilling of the filter. In addition, a deeper hole was obtained in borosilicate glass at the pulse repetition rate of 20 kHz ( $\sim 1120$   $\mu\text{m}$  as seen in Fig. 8c); therefore, particle scattering is not seen prominently in Fig. 9. Particle shielding, however, may be prominent with deeper hole drilling or higher repetition rates.

Evaporating materials absorb the laser beam and become plasma. This plasma absorbs and scatters the laser light, and hence an attenuated beam arrives at the bottom of the hole. For low ionization densities, the absorption coefficient is given by the Drude theory. With high ionization, the coefficient follows from the Kramers–Unsöld equation for inverse Bremsstrahlung [31]. Breitling et al. [23] obtained values experimentally for the absorption coefficient of plasma formed by the laser ablation of  $\text{Si}_3\text{N}_4$  at wavelengths of 1064, 532, and 355 nm. They reported that the absorption coefficient decreases in the short-wavelength regime. In this report, a short-wavelength laser beam was used in illuminations and suppressed the plasma shielding enabled an effective delivery of the beam to the bottom of the hole and hence deeper hole drilling.

## 5 Conclusion

High-aspect-ratio microdrilling was performed, and the reduction in the ablation threshold in glass caused by heat accumulation was studied.

First, the dependence on pulse repetition frequency of the ablation threshold at the glass surface was studied experimentally and numerically. It was confirmed that the pulse repetition rate affected markedly both the heat accumulation and temperature. For example, no change was observed at pulse energies below 1  $\mu\text{J}$  at a rate of 1 kHz; in contrast, melting was observed at 0.3  $\mu\text{J}$ , and ablation occurred at 0.7  $\mu\text{J}$  for the 20-kHz pulse repetition rate.

Second, the dependences on pulse repetition rate of hole depth and of the fluences within a drilled hole were analyzed and discussed. The hole depth obtained was

$\sim 250$   $\mu\text{m}$  for the pulse repetition rate of 1 kHz and was 500  $\mu\text{m}$  for the pulse repetition rate of 20 kHz. The laser energy at the bottom of the hole was estimated from the energy emitted from a through-hole. A fluence of  $\sim 4$   $\text{J}/\text{cm}^2$  observed for the pulse repetition rate of 1 kHz decreased to 1  $\text{J}/\text{cm}^2$  for the pulse repetition rate of 20 kHz.

**Acknowledgments** The authors gratefully acknowledge the support of the Advanced Machining Technology and Development Association (AMTDA) and the Japan Science and Technology Agency (JST) under the Development of Innovative Seeds, Potentiality Verification Stage.

## References

- Z.L. Li, T.T. Lin, P.M. Moran, *Appl. Phys. A* **81**, 753 (2005)
- A. Ancona, F. Roser, K. Rademaker, J. Limpert, S. Nolte, A. Tünnermann, *Opt. Express* **16**, 8958 (2008)
- F. Brygo, A. Semerok, R. Oltra, J.M. Weulersse, S. Fomichev, *Appl. Surf. Sci.* **252**, 8314 (2006)
- S. Hiramoto, M. Moriyasu, S. Takeno, Effect of beam-plasma interaction on characteristics of drilling: study on materials processing by high peak short pulse  $\text{CO}_2$  laser (Report 2). Q. J. Jpn. Weld. Soc. **11**, 75 (1993)
- J. Finger, M. Reininghaus, *Opt. Express* **22**, 18790 (2014)
- A. Weck, T.H.R. Crawford, D.S. Wilkinson, H.K. Haugen, J.S. Preston, *Appl. Phys. A* **90**, 537 (2008)
- F. Di Niso, C. Gaudio, T. Sibillano, F.P. Mezzapesa, A. Ancona, P.M. Lugarà, *Opt. Express* **22**, 12200 (2014)
- R. Weber, T. Graf, P. Berger, V. Onuseit, M. Wiedenmann, C. Freitag, A. Feuer, *Opt. Express* **22**, 11312 (2014)
- C.B. Schaffer, J.F. García, E. Mazur, *Appl. Phys. A* **76**, 351 (2003)
- S. Karimelahi, L. Abolghasemi, P. Herman, *Appl. Phys. A* **114**, 91 (2014)
- S. Eaton, H. Zhang, P. Herman, F. Yoshino, L. Shah, J. Bovatsek, A. Arai, *Opt. Express* **13**, 4708 (2005)
- S. Richter, S. Döring, A. Tünnermann, S. Nolte, *Appl. Phys. A* **103**, 257 (2011)
- T. Tamaki, W. Watanabe, K. Itoh, *Opt. Express* **14**, 10460 (2006)
- C. S. Nielsen, P. Balling, *J. Appl. Phys.* **99**, 093101 (2006)
- S. Döring, J. Szilagy, S. Richter, F. Zimmermann, M. Richardson, A. Tünnermann, S. Nolte, *Opt. Express* **20**, 27147 (2012)
- S. Döring, T. Ullsperger, F. Heisler, S. Richter, A. Tünnermann, S. Nolte, *Phys. Procedia* **41**, 431 (2013)
- D. Esser, S. Rezaei, J. Li, P.R. Herman, J. Gottmann, *Opt. Express* **19**, 25632 (2011)
- L. Shah, J. Tawney, M. Richardson, K. Richardson, *Appl. Surf. Sci.* **183**, 151 (2001)
- A. Salleo, T. Sands, F.Y. Genin, *Appl. Phys. A* **71**, 601 (2000)
- D.J. Hwang, T.Y. Choi, C.P. Grigoropoulos, *Appl. Phys. A* **79**, 605 (2004)
- X. Zhao, Y. Shin, *Appl. Phys. A Mater. Sci. Process.* **104**, 713 (2011)
- C. Hnatovsky, R.S. Taylor, E. Simova, P.P. Rajeev, D.M. Rayner, V.R. Bhardwaj, P.B. Corkum, *Appl. Phys. A* **84**, 47 (2006)
- D. Breitling, H. Schittenhelm, P. Berger, F. Dausinger, H. Hugel, *Proc. SPIE* **4184**, 534 (2001)
- Personal communication, Provided by the manufacturer
- R.I. Golyatina, A.N. Tkachev, S.I. Yakovlenko, *Laser Phys.* **14**, 1429 (2004)
- S.I. Yakovlenko, *Laser Phys.* **16**, 1273 (2006)

27. Schott datasheet, [http://edit.schott.com/advanced\\_optics/english/abbe\\_datasheets/schott\\_datasheet\\_n-bk7.pdf](http://edit.schott.com/advanced_optics/english/abbe_datasheets/schott_datasheet_n-bk7.pdf). Accessed 24 January 2015
28. R.R. Gattass, L.R. Cerami, E. Mazur, *Opt. Express* **14**, 5279 (2006)
29. M.B. Volf, *Chemical approach to glass* (Elsevier, Amsterdam, 1984)
30. J.E. Shelby, *Introduction to glass science and technology*, 2nd edn. (Royal Society of Chemistry, Cambridge, 2005)
31. D. Baeuerle, *Laser Processing and Chemistry*, 3rd edn. (Springer, New York, 2000)